American Mineralogist, Volume 98, pages 478–484, 2013

Scottyite, the natural analog of synthetic $BaCu_2Si_2O_7$, a new mineral from the Wessels mine, Kalahari Manganese Fields, South Africa

Hexiong Yang,[1,*] Robert T. Downs,[1] Stanley H. Evans,[1] and William W. Pinch[2]

[1]Department of Geosciences, University of Arizona, Tucson, Arizona 85721-0077, U.S.A.
[2]19 Stonebridge Lane, Pittsford, New York 14534, U.S.A.

Abstract

A new mineral species, scottyite, ideally $BaCu_2Si_2O_7$, has been found in the Wessels mine, Kalahari Manganese Fields, Northern Cape Province, South Africa. The mineral appears to have formed as a result of a hydrothermal event and is associated with wesselsite, pectolite, richterite, sugilite, and lavinskyite. Scottyite forms blocky grains with striations parallel to the **c** axis. Crystals are found up to 0.4 × 0.3 × 0.3 mm. No twinning is observed. The mineral is dark-blue in transmitted and under incident lights, transparent with pale blue streak and vitreous luster. It is brittle and has a Mohs hardness of 4~5; cleavage is perfect on {100} and {010} and no parting was observed. The calculated density is 4.654 g/cm^3. Optically, scottyite is biaxial (–), with α = 1.750(1), β = 1.761(1), and γ = 1.765(1), $2V_{meas}$ = 66(2)°. It is insoluble in water, acetone, or hydrochloric acid. An electron microprobe analysis produced an average composition (wt%) (8 points) of CuO 36.98(31), BaO 35.12(16), SiO_2 27.01(61), SrO 0.28(5), and Na_2O 0.06(2), and total = 99.45(65), yielding an empirical formula (based on 7 O apfu) $Ba_{1.00}Sr_{0.01}Na_{0.01}Cu_{2.04}Si_{1.97}O_7$.

Scottyite is the natural analog of synthetic $BaCu_2(Si,Ge)_2O_7$, which exhibits novel one-dimensional quantum spin-1/2 antiferromagnetic properties with tunable super-exchange interactions. It is orthorhombic, with space group *Pnma* and unit-cell parameters a = 6.8556(2), b = 13.1725(2), c = 6.8901(1) Å, and V = 622.21(6) Å^3. The structure of scottyite is characterized by flattened CuO_4 tetrahedra sharing corners with one another to form chains parallel to the **c** axis. These chains are interlinked by Si_2O_7 tetrahedral dimers and Ba^{2+}. The Ba^{2+} cations are bonded to seven O atoms in an irregular coordination. The average Si-O, Cu-O, and Ba-O bond lengths are 1.630, 1.941, and 2.825 Å, respectively. Scottyite is topologically related to a group of compounds with the general formula $BaM_2^{2+}Si_2O_7$, where M = Be (barylite and clinobarylite), Fe (andrémeyerite), Mg, Mn, Co, and Zn.

Keywords: Scottyite, $BaCu_2Si_2O_7$, crystal structure, X-ray diffraction, Raman spectra

Introduction

A new mineral species, scottyite, ideally $BaCu_2Si_2O_7$, has been found in the Wessels mine, Kalahari Manganese Fields, Northern Cape Province, Republic of South Africa. It is named after Michael M. Scott "Scotty", the co-founder and first CEO of Apple Computer Corporation (February 1977 to March 1981), and the founding sponsor of the RRUFF project—an internet-based, internally consistent, and integrated database of Raman spectra, X ray diffraction, and chemistry data for minerals. The vivid color of the mineral reflects his spectroscopic interests, and the synthetic analog's high-tech applications mirror his role in introducing the desktop computer to the world. The new mineral and its name have been approved by the Commission on New Minerals, Nomenclature and Classification (CNMNC) of the International Mineralogical Association (IMA 2012-027). Part of the co-type sample has been deposited at the University of Arizona Mineral Museum (Catalog no. 19334) and the RRUFF Project (deposition no. R120077) (http://www.webcitation.org/6C98YyC9g). The holotype sample is in the collection of W.W. Pinch.

Silicates with only Ba and Cu as essential structural constituents are relatively rare in nature and only two such minerals have been documented thus far, including effenbergerite $BaCuSi_4O_{10}$ (Giester and Rieck 1994) and scottyite, both originating from the same locality. Nevertheless, Ba-silicate compounds characterized by the general chemical formula $BaM_2^{2+}Si_2O_7$ (M^{2+} = Be, Mg, Mn, Fe, Co, Zn, and Cu) have been a subject of extensive investigations for their scientific and industrial interests. For example, the materials with M = Be, Mg, and Zn are suitable hosts for luminescent activating ions. In particular, Pb^{2+}-doped $BaBe_2Si_2O_7$ is used commercially as a UV emitting material in moth-killing lamps and (Eu^{2+} + Mn^{2+})-doped $BaMg_2Si_2O_7$ is a deep-red luminescent emitter through effective energy transfers from Eu^{2+} to Mn^{2+} (Barry 1970; Yao et al. 1998). Moreover, compounds with M = Cu, Co, and Mn are ideal prototypical quasi-one-dimensional quantum spin (=1/2, 3/2, and 5/2, respectively) Heisenberg antiferromagnets with adjustable superexchange interactions, which is vital for our understanding of high-*Tc* superconductivity (e.g., Janczak et al. 1990; Adams and Layland 1996; Lu et al. 2000; Yamada

* E-mail: hyang@u.arizona.edu

0003-004X/13/0203–478$05.00/DOI: http://dx.doi.org/10.2138/am.2013.4326

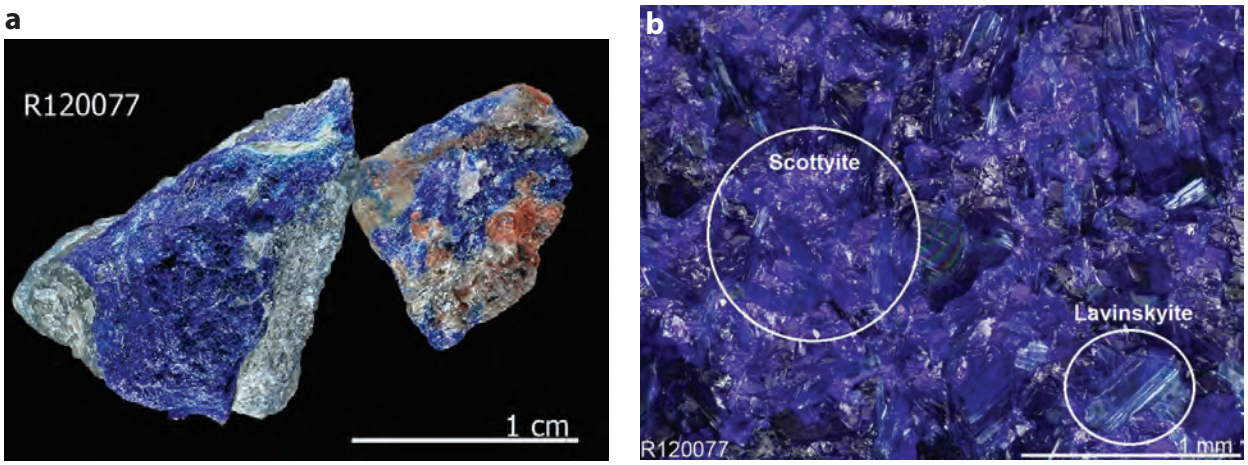

FIGURE 1. (**a**) Rock samples on which scottyite crystals are found. (**b**) A microscopic view of scottyite, associated with light blue platy lavinskyite. (Color online.)

et al. 2001a, 2001b; Ohta et al. 2004a, 2004b; Bertaina and Hayn 2006; Zvyagin 2006; Zheludev et al. 2007). Among the $BaM_2^{2+}Si_2O_7$ family, the Be- and Fe-bearing members have been found in nature, namely barylite, clinobarylite, and andrémeyerite. This paper describes the physical and chemical properties of scottyite and its crystal structure determined from the single-crystal X-ray diffraction data, demonstrating that scottyite is the natural analog to the synthetic Cu-member of the $BaM_2^{2+}Si_2O_7$ family.

SAMPLE DESCRIPTION AND EXPERIMENTAL METHODS

Occurrence, physical, and chemical properties, and Raman spectra

Scottyite was found on two specimens originating from the central-eastern ore body of the Wessels mine, Kalahari Manganese Fields, Northern Cape Province, Republic of South Africa. It is in a massive assemblage associated with wesselsite $SrCuSi_4O_{10}$, lavinskyite $K(LiCu)Cu_6Si_8O_{22}(OH)_4$, pectolite $NaCa_2Si_3O_8(OH)$, richterite $Na(CaNa)Mg_5Si_8O_{22}(OH)_2$, and sugilite $KNa_2Fe_2^{3+}(Li_3Si_{12})O_{30}$ (Figs. 1 and 2). The mineral assemblage probably formed as a result of a hydrothermal event. Conditions during metamorphism were in the range of 270–420 °C at 0.2–1.0 kbar (Kleyenstuber 1984; Gutzmer and Beukes 1996). Detailed reviews on the geology and mineralogy of the Kalahari Manganese Fields have been given by Kleyenstuber (1984), Von Bezing et al. (1991), and Gutzmer and Beukes (1996). It should be pointed out that scottyite was actually first reported as an unnamed Ba-Cu silicate from Eifel, Germany (Hentschel 1993; Blass et al. 2009; Blass and Schüller 2011). However, this unnamed mineral was not fully described and documented in the list of the IMA valid or invalid unnamed minerals. Since scottyite was approved as a new mineral species based on our mineralogical data, we consider the Wessels Mine, South Africa, rather than Eifel, Germany, as its type locality.

Scottyite forms blocky grains with striations parallel to the **c** axis. Crystals are found up to 0.4 × 0.3 × 0.3 mm. No twinning is observed. The mineral is dark blue, transparent with pale blue streak and vitreous luster. It is brittle and has a Mohs hardness of 4~5; cleavage is perfect on {100} and {010} and no parting was observed. The measured and calculated densities are 4.63(3) and 4.654 g/cm^3, respectively. Optically, scottyite is biaxial (–), with α = 1.750(1), β = 1.761(1), γ = 1.765(1) (white light), $2V$ (meas) = 66(2)°, $2V$ (calc) = 62°, and the orientation X || **a**, Y || **b**, Z || **c**. The pleochroism is X = medium blue, Y = dark blue, and Z = medium blue, and the absorption $Y > X = Z$. No dispersion was observed. Scottyite is insoluble in water, acetone, or hydrochloric acid.

The chemical composition was determined using a CAMECA SX-100 electron microprobe (15 kV, 20 nA, < 1 μm beam diameter) (http://rruff.info/scottyite). The standards used included chalcopyrite (Cu), NBS_K458 (Ba), diopside (Si), $SrTiO_3$ (Sr), and albite (Na), yielding an average composition (wt%) (8 points) of CuO 36.98(31), BaO 35.12(16), SiO_2 27.01(61), SrO 0.28(5), and Na_2O 0.06(2), and total = 99.45(65). The resultant chemical formula, calculated on the basis of 7 O apfu (from the structure determination), is $Ba_{1.00}Sr_{0.01}Na_{0.01}Cu_{2.04}Si_{1.97}O_7$, which can be simplified to $BaCu_2Si_2O_7$.

The Raman spectrum of scottyite was collected on a randomly oriented crystal from 12 scans at 60 s and 100% power per scan on a Thermo-Almega microRaman system, using a solid-state laser with a wavelength of 532 nm and a thermoelectric cooled CCD detector. The laser is partially polarized with 4 cm^{-1} resolution and a spot size of 1 μm.

X-ray crystallography

Because of the limited amount of available material, no powder X-ray diffraction data were measured for scottyite. Listed in Table 1 are the powder X-ray diffraction data calculated from the determined structure using the program XPOW (Downs et al. 1993). Single-crystal X-ray diffraction data of scottyite were collected from a nearly equi-dimensional, untwinned crystal (0.04 × 0.05 × 0.05 mm) with frame widths of 0.5° in ω and 30 s counting time per frame. All reflections were indexed on the basis of an orthorhombic unit-cell (Table 2). The intensity data were corrected for X-ray absorption using the Bruker program SADABS. The systematic absences of reflections suggest possible space groups *Pnma* (no. 62) or $Pn2_1a$ (no. 33). The crystal structure was solved and refined using SHELX97 (Sheldrick 2008) based on the space group *Pnma*, because it

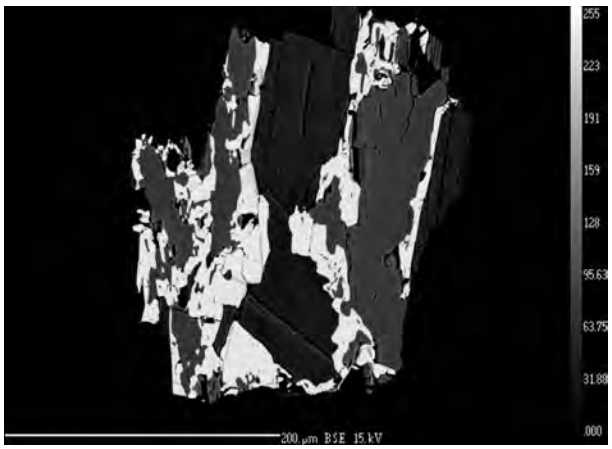

FIGURE 2. A backscattered electron image, showing the assemblage of scottyite (bright), wesselsite (gray), and lavinskyite (dark gray).

TABLE 1. Calculated powder X-ray diffraction data for scottyite

Intensity	d_{calc}	*h k l*
51.70	6.5862	0 2 0
1.46	6.1053	0 1 1
4.92	4.8598	1 0 1
21.96	3.9105	1 2 1
1.50	3.7029	0 3 1
2.03	3.3173	2 1 0
10.74	3.2931	0 4 0
16.92	3.0782	1 0 2
5.41	3.0690	2 0 1
63.84	3.0527	0 2 2
100.00	3.0406	2 2 0
5.41	2.9975	1 1 2
2.09	2.9889	2 1 1
12.31	2.7887	1 2 2
11.74	2.7818	2 2 1
51.65	2.7262	1 4 1
3.38	2.5205	1 3 2
10.71	2.5154	2 3 1
1.94	2.4608	0 5 1
37.15	2.4299	2 0 2
1.05	2.3896	2 1 2
5.44	2.3805	0 4 2
16.44	2.3748	2 4 0
4.61	2.3161	1 5 1
1.56	2.2797	2 2 2
3.74	2.2626	0 1 3
2.99	2.2488	1 4 2
2.95	2.2452	2 4 1
1.42	2.1954	0 6 0
1.18	2.1690	3 0 1
1.96	2.1486	1 1 3
2.15	2.1261	2 3 2
2.02	2.0888	2 5 0
4.78	2.0676	1 2 3
4.27	2.0602	3 2 1
5.06	2.0007	1 6 1
20.52	1.9552	2 4 2
1.20	1.9510	1 3 3
2.18	1.9080	2 0 3
2.43	1.9043	3 0 2
5.18	1.8847	3 1 2
12.93	1.8514	0 6 2
15.11	1.8487	2 6 0
2.53	1.8294	3 2 2
3.04	1.8165	1 4 3
5.90	1.8114	3 4 1
6.35	1.7874	1 6 2
2.24	1.7499	2 3 3
4.88	1.7225	0 0 4
7.82	1.7139	4 0 0
6.96	1.6706	1 0 4
4.51	1.6573	1 1 4
2.72	1.6485	3 4 2
11.99	1.6466	0 8 0
4.77	1.6290	2 6 2
10.00	1.6193	1 2 4
3.70	1.6126	4 2 1
1.18	1.5614	1 3 4
2.11	1.5461	1 6 3
2.64	1.5453	2 5 3
5.94	1.5430	3 6 1
2.92	1.5203	4 4 0
4.65	1.4987	2 2 4
9.34	1.4945	4 2 2
6.31	1.4899	1 4 4
7.26	1.4846	4 4 1
1.11	1.4556	0 7 3
10.60	1.4536	3 4 3
3.65	1.4519	1 8 2
1.19	1.4386	3 6 2
3.42	1.3943	2 4 4
2.79	1.3909	4 4 2
1.63	1.3755	3 0 4
2.46	1.3681	3 1 4
14.20	1.3631	2 8 2
4.20	1.3465	3 2 4

TABLE 2. Summary of crystal data and refinement results for scottyite and synthetic $BaCu_2Si_2O_7$

	Scottyite	Synthetic $BaCu_2Si_2O_7$
Ideal chemical formula	$BaCu_2Si_2O_7$	$BaCu_2Si_2O_7$
Crystal symmetry	Orthorhombic	Orthorhombic
Space group	*Pnma* (no.62)	*Pnma* (no.62)
a (Å)	6.8556(2)	6.866(2)
b (Å)	13.1725(2)	13.190(3)
c (Å)	6.8901(1)	6.909(2)
V (Å^3)	622.21(6)	627.7(3)
Z	4	4
ρ_{cal} (g/cm^3)	4.654	4.592
λ (Å, Mo*K*α)	0.71073	0.71069
μ (mm^{-1})	13.41	13.75
2θ range for data collection	≤65.12	60.0
No. reflections collected	4887	
No. independent reflections	1180	
No. reflections with $I > 2\sigma(I)$	1065	1039
No. parameters refined	59	59
R_{int}	0.023	0.028
Final R_1, wR_2 factors [$I > 2\sigma(I)$]	0.017, 0.040	0.031, 0.037
Final R_1, wR_2 factors (all data)	0.021, 0.041	
Goodness-of-fit	1.074	
Reference	This study	Janczak et al. (1990)

yielded better refinement statistics in terms of bond lengths and angles, atomic displacement parameters, and *R* factors. The positions of all atoms were refined with anisotropic displacement parameters. During the structure refinements, the ideal chemistry was assumed, as the overall effects of the trace amounts of other elements (Sr and Na) on the final structure results are negligible. Final coordinates and displacement parameters of atoms in scottyite are listed in Table 3, and selected bond-distances in Table 4. (A CIF[1] is on deposit.)

DISCUSSION

Crystal structure

Scottyite is identical with synthetic $BaCu_2Si_2O_7$ (Janczak et al. 1990; Yamada et al. 2001a) and isostructural with $BaCu_2Ge_2O_7$ (Oliveira 1993; Yamada et al. 2001a). Our structure data agree well with those determined for synthetic $BaCu_2Si_2O_7$ by Janczak et al. (1990) using single-crystal X-ray diffraction (Tables 2 and 4). The structure of scottyite is based on a tetrahedral framework consisting of SiO_4 and CuO_4 tetrahedra. The CuO_4 tetrahedra are considerably flattened and share corners to form chains parallel to the **c** axis. The chains are interlinked by the Si_2O_7 dimers oriented parallel to the **b** axis. The Ba^{2+} cations are in the framework channels (Fig. 3). The Cu-O-Cu angle within the CuO_4 tetrahedral chain is 124.49°, which is responsible for the antiferromagnetic coupling in $BaCu_2Si_2O_7$ (Yamada et al. 2001a).

The Ba^{2+} cation in scottyite is bonded to seven O atoms within 3.0 Å in an irregular coordination. The next two nearest O atoms (O4) are 3.263 Å away. The bond-valence sum for Ba^{2+}, calculated using the parameters given by Brese and O'Keeffe (1991), is only 1.69 v.u. (Table 5), indicating that it is significantly under-bonded (Table 5). In contrast, the Ba^{2+} cations in effenbergerite are bonded to eight O atoms in a distorted cube coordination with a bond-valence sum of 1.95 v.u. (Chakoumakos et al. 1993; Giester and Rieck 1994). The Cu^{2+} cations

[1] Deposit item AM-13-030, CIF. Deposit items are available two ways: For a paper copy contact the Business Office of the Mineralogical Society of America (see inside front cover of recent issue) for price information. For an electronic copy visit the MSA web site at http://www.minsocam.org, go to the *American Mineralogist* Contents, find the table of contents for the specific volume/issue wanted, and then click on the deposit link there.

TABLE 3. Coordinates and displacement parameters of atoms in scottyite

Atom	*x*	*y*	*z*	U_{eq}	U_{11}	U_{22}	U_{33}	U_{23}	U_{13}	U_{12}
Ba	0.01303(2)	1/4	0.45688(3)	0.00970(5)	0.0089(1)	0.0108(1)	0.0095(1)	0	−0.0008(1)	0
Cu	0.27762(4)	0.00417(2)	0.20631(4)	0.00714(6)	0.0089(1)	0.0057(1)	0.0068(1)	−0.0008(1)	−0.0023(1)	0.0014(1)
Si	0.49765(7)	0.13406(5)	0.52716(8)	0.0057(1)	0.0066(2)	0.0047(2)	0.0057(3)	−0.0000(2)	0.0004(2)	0.00039(2)
O1	0.4044(3)	1/4	0.5167(3)	0.0087(4)	0.0084(9)	0.0057(9)	0.0120(9)	0	−0.0004(8)	0
O2	0.1725(2)	0.1337(1)	0.1306(2)	0.0104(3)	0.0122(6)	0.0068(7)	0.0122(7)	−0.0003(6)	−0.0053(6)	0.0022(5)
O3	0.5590(2)	0.1121(1)	0.7486(2)	0.0111(3)	0.0152(7)	0.0098(7)	0.0083(7)	−0.0017(6)	−0.0031(6)	0.0048(6)
O4	0.3173(2)	0.0596(1)	0.4658(2)	0.0078(3)	0.0105(6)	0.0076(7)	0.0053(6)	−0.0010(5)	0.0007(5)	−0.0022(5)

TABLE 4. Selected bond distances (Å) in scottyite and synthetic $BaCu_2Si_2O_7$

	Scottyite	Synthetic $BaCu_2Si_2O_7$
Ba-O1	2.715(2)	2.713(5)
Ba-O2 x2	2.857(2)	2.863(3)
Ba-O2 x2	2.932(2)	2.932(3)
Ba-O3	2.741(2)	2.749(3)
Avg.	2.825	2.830
Cu-O2	1.924(2)	1.930(3)
Cu-O3	1.923(2)	1.926(2)
Cu-O4	1.950(2)	1.956(2)
Cu-O4	1.968(2)	1.973(3)
Avg.	1.941	1.946
Si-O1	1.657(1)	1.662(2)
Si-O2	1.618(2)	1.619(4)
Si-O3	1.609(2)	1.610(4)
Si-O4	1.634(2)	1.635(3)
Avg.	1.630	1.632

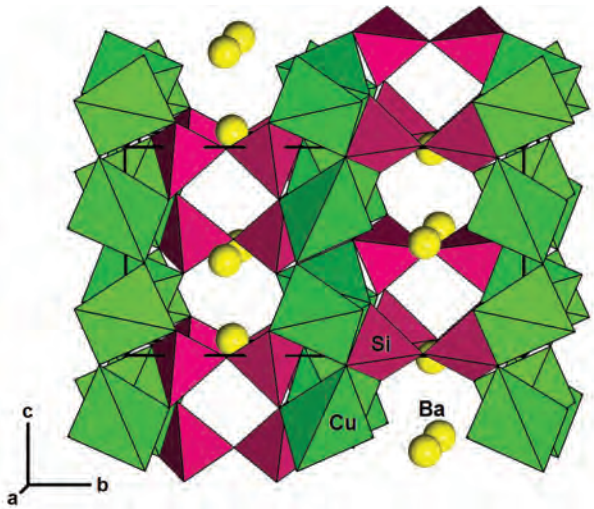

FIGURE 3. Crystal structure of scottyite. (Color online.)

in both scottyite and effenbergerite, however, exhibit a similar, nearly planar square coordination. The difference between the Cu coordinations in the two minerals is that the four O atoms bonded to Cu^{2+} in effenbergerite lie in the same plane, with Cu^{2+} slightly (0.67 Å) off the plane (Giester and Rieck 1994), whereas they form a markedly flattened tetrahedron in scottyite. The similar planar or nearly planar square coordinations for Cu^{2+} have also been observed in other synthetic Ba-Cu-silicates, such as $I\bar{4}m2$ $BaCuSi_2O_6$ (Finger et al. 1989), as well as $I4_1/acd$ and $I4/mmm$ $BaCuSi_2O_6$ (Sparta and Roth 2004).

The Si-O-Si angle within the Si_2O_7 dimer in scottyite is 134.3°, which is the second largest in the $BaM_2^{2+}Si_2O_7$ group,

TABLE 5. Calculated bond-valence sums for scottyite

	O1	O2	O3	O4	Sum
Ba	0.317	0.216×2→ 0.176×2→	0.296×2→		1.693
Cu		0.516	0.517	0.481 0.458	1.972
Si	0.915×2↓	1.016	1.041	0.973	3.945
Sum	2.147	1.924	1.854	1.912	

only smaller than that in clinobarylite (138.5°) (Table 6). However, an examination of the clinobarylite structure (Krivovichev et al. 2004) reveals a peculiar feature: the Si-O_{br} (bridging O atom) distance (1.597 Å) is significantly shorter than the Si-O_{nbr} (non-bridging O atoms) distances (1.619–1.631 Å). This contradicts the previous observations for disilicate compounds (e.g., Lin et al. 1999; Fleet and Liu 2001; Kolitsch et al. 2009), including all other compounds in the $BaM_2^{2+}Si_2O_7$ group. Our redetermination of the clinobarylite structure with a crystal from the type locality (Khibiny Massif, Kola Peninsula, Rassia) confirmed its true space group $Pmn2_1$ ($R_1 = 0.011$ and $R_w = 0.026$), as that reported by Krivovichev et al. (2004), but yielded the Si-O_{br} length of 1.657(1) Å and the Si-O-Si angle of 128.82(8)° (Di Domizio et al. 2012). Regardless, the Si-O-Si angles for the compounds in the $BaM_2^{2+}Si_2O_7$ group are among the smallest of disilicate materials, which generally exhibit Si-O-Si angles ranging from 120 to 180° (Lin et al. 1999; Fleet and Liu 2001; Kolitsch et al. 2009 and references therein).

There is a strong resemblance in the structural topology among the $BaM_2^{2+}Si_2O_7$ compounds, despite their diverse structural symmetries (Table 6): they are all composed of corner-shared MO_4 tetrahedral chains that are interlinked by Si_2O_7 tetrahedral dimers and Ba^{2+} cations. The major differences among these compounds consist in the relative arrangements of Ba^{2+} and Si_2O_7 with respect to the MO_4 tetrahedral chains, thus giving rise to different coordination environments around Ba^{2+} and M^{2+}. For example, the Ba^{2+} cation is only coordinated by five O atoms in high-temperature $Ccm2_1$ $BaZn_2Si_2O_7$, but seven in scottyite, and nine in barylite and clinobarylite. Moreover, there is only one type of symmetrically distinct MO_4 tetrahedra in scottyite, barylite, clinobarylite, and high-temperature $Ccm2_1$ $BaZn_2Si_2O_7$, but two in andrémeyerite, and three in $C2/c$ compounds in the $BaM_2^{2+}Si_2O_7$ group.

Raman spectra

The Raman spectrum of scottyite is plotted in Figure 4, along with the spectra of barylite and clinobarylite (R060620 and R060606, respectively, from the RRUFF Project) for comparison. Based on previous experimental and theoretical Raman spectroscopic studies on various disilicate compounds (e.g., Sharma et al. 1988; Fleet and Henderson 1997; Makreski et al. 2007; Kaminskii et al. 2011; Becker et al. 2012), we made

TABLE 6. Comparison of crystallographic data for $BaM_2Si_2O_7$-type minerals and compounds

	Chemical formula	Space group	Unit-cell parameters				Si-O-Si (°)	Ba-coordination	Reference
			a (Å)	*b* (Å)	*c* (Å)	β (°)			
Scottyite	$BaCu_2Si_2O_7$	*Pnma*	6.8556	13.1725	6.8901		134.3	7	(1)
Barylite	$BaBe_2Si_2O_7$	*Pnma*	9.820	11.670	4.690		128.6	9	(2)
Clinobarylite	$BaBe_2Si_2O_7$	$Pmn2_1$	11.650	4.922	4.674		138.5	9	(3)
Clinobarylite	$BaBe_2Si_2O_7$	$Pnm2_1$	4.9175	11.6491	4.6746		128.8	9	(9)
Andremeyerite	$BaFe_2Si_2O_7$	$P2_1/c$	7.488	13.785	7.085	118.23	127.2	7	(4)
Synthetic	$BaCo_2Si_2O_7$	*C2/c*	7.2131	12.781	13.762	90.299	124.5	8	(5)
Synthetic	$BaMg_2Si_2O_7$	*C2/c*	7.2455	12.7138	13.7481	90.211	125.2	7	(6)
Synthetic	$BaMn_2Si_2O_7$	*C2/c*	7.2953	12.9632	14.0321	90.248	no data		(7)
Synthetic	$BaZn_2Si_2O_7$-25°C	*C2/c*	7.2782	12.8009	13.6869	90.093	124.8	8	(8)
Synthetic	$BaZn_2Si_2O_7$-280 °C	$Ccm2_1$	7.6199	13.0265	6.7374		131.7	5	(8)

Notes: The *a* and *b* axis for clinobarylite were switched in our structure refinement to facilitate a direct comparison with the unit-cell setting for barylite. References: (1) This work; (2) Robinson and Fang (1977); (3) Krivovichev et al. (2004); (4) Cannillo et al. (1988); (5) Adams and Layland (1996); (6) Park and Choi (2009); (7) Lu et al. (2000); (8) Lin et al. (1999); (9) Di Domizio et al. (2012).

a tentative assignment of major Raman bands for scottyite (Table 7). Evidently, the Raman spectra of scottyite, barylite, and clinobarylite are quite similar. In general, they can be divided into four regions. Region 1, between 800 and 1100 cm^{-1}, contains bands attributable to the Si-O symmetric and anti-symmetric stretching vibrations (ν_1 and ν_3 modes) within the SiO_4 tetrahedra. Region 2, between 660 and 700 cm^{-1}, includes bands resulting from the Si-O_{br}-Si bending vibrations within the Si_2O_7 tetrahedral dimers. Major bands in region 3, ranging from 420 to 660 cm^{-1}, are ascribed to the O-Si-O symmetric and anti-symmetric bending vibrations (ν_2 and ν_4 modes) within the SiO_4 tetrahedra. The bands in region 4, below 420 cm^{-1}, are mainly associated with the rotational and translational modes of SiO_4 tetrahedra, as well as the Cu-O interactions and lattice vibrational modes.

One of the noticeable features in Figure 4 is that the wavenumbers of the bands due to the Si-O_{br}-Si bending mode for barylite and clinobarylite are nearly identical (~685 cm^{-1}), indicating that the Si-O_{br} bond lengths and the Si-O_{br}-Si angles in these two minerals are comparable. This is indeed the case. The Si-O_{br} distance and the Si-O_{br}-Si angle are 1.657 Å and 128.59°, respectively, in barylite (Robinson and Fang 1977), and 1.657 Å and 128.82° in clinobarylite (Di Domizio et al. 2012). For scottyite, the corresponding band occurs at a wavenumber (674 cm^{-1}) smaller than that for barylite or clinobarylite. This shift is mostly related to the larger Si-O_{br}-Si angle in scottyite, as the Si-O_{br} bond length in scottyite is identical to that in barylite or clinobarylite. A similar correlation between the positions of the bands stemming from the Si-O_{br}-Si bending vibrations and the Si-O_{br}-Si angles has also been observed in chain silicates with the same or similar structures (Huang et al. 2000 and references therein).

Ba-Sr distribution between scottyite and wesselsite

As shown in Figure 2, scottyite is intimately associated with wesselsite and lavinskyite. The chemical composition

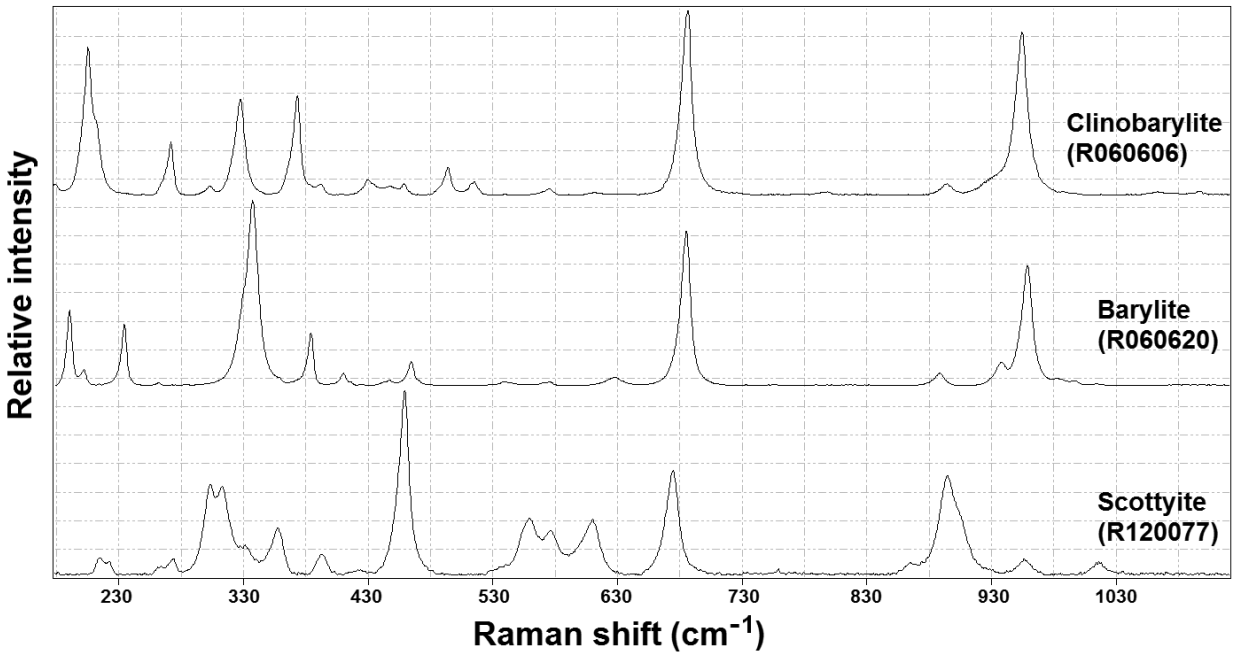

FIGURE 4. Raman spectra of scottyite, barylite, and clinobarylite. The spectra are shown with vertical offset for more clarity.

TABLE 7. Tentative assignments of major Raman bands for scottyite

Bands (cm^{-1})	Intensity	Assignment
1019, 958, 866	Relatively weak	ν_3 (SiO_4) anti-symmetric stretching
896	Strong, sharp	ν_1 (SiO_4) symmetric stretching
675	Strong, sharp	Si-O-Si bending
612, 578, 560	Relatively strong, sharp	ν_4 (SiO_4) anti-symmetric bending
459	Very strong, sharp	ν_2 (SiO_4) symmetric bending
<420	Strong to weak	SiO_4 rotational modes, lattice vibrational modes, and Cu-O interactions

of wesselsite in our sample, determined under the same experimental conditions as those for scottyite, is $(Sr_{0.98}Ba_{0.04})_{\Sigma=1.02}Cu_{1.05}Si_{3.97}O_{10}$ (the average of 10 analysis points). Wesselsite is isostructural with effenbergerite ($BaCuSi_4O_{10}$) (Chakoumakos et al. 1993; Giester and Rieck 1994, 1996), and a complete solid solution between them, $(Sr,Ba)CuSi_4O_{10}$, has been observed experimentally (Knight et al. 2010). Very intriguingly, while wesselsite in our sample contains little Ba, scottyite contains essentially no Sr. Thus far, no compound with the composition $SrCu_2Si_2O_7$ has been reported. In fact, there is no documentation for any $SrM_2Si_2O_7$ compounds. It then begs the question whether scottyite in particular and the $BaM_2Si_2O_7$ compounds in general are capable of accommodating a significant amount of smaller Sr^{2+}. [The radii of Ba^{2+} and Sr^{2+} in eightfold coordination are 1.42 and 1.26 Å, respectively (Shannon 1976).] As described above, the Ba^{2+} cations in the $BaM_2Si_2O_7$ compounds are situated in the cavities in the framework formed by the Si_2O_7 dimers and the MO_4 tetrahedral chains. Conceivably, any substantial replacement of large Ba^{2+} by smaller Sr^{2+} would require, in addition to the other structural adjustments (such as the tilting or distortion of MO_4 and/or SiO_4 tetrahedra), further narrowing of the Si-O-Si angles in the Si_2O_7 dimers to better satisfy the bonding environment for Sr^{2+}. This, however, would not be energetically favorable, because the Si-O-Si angles in the $BaM_2Si_2O_7$ compounds are already among the smallest of disilicate materials. For scottyite, the Ba^{2+} cation is appreciably underbonded (Table 5), suggesting that the current framework is unable to provide it with a tighter bond environment through additional distortion. Accordingly, any sizable substitution of Sr^{2+} for Ba^{2+} would worsen the bonding energetics for this site and thus destabilize the entire structure. Nevertheless, we cannot rule out the possible existence of $SrM_2Si_2O_7$ compounds at different conditions, such as under high pressures.

ACKNOWLEDGMENTS

This study was funded by the Science Foundation Arizona.

REFERENCES CITED

Adams, R.D. and Layland, R. (1996) Syntheses, structural analyses, and unusual magnetic properties of $Ba_2CoSi_2O_7$ and $BaCo_2Si_2O_7$. Inorganic Chemistry, 35, 3492–3497.

Barry, T.L. (1970) Luminescent properties of Eu^{2+} and Eu^{2+} + Mn^{2+} activated $BaMg_2Si_2O_7$. Journal of Electrochemical Society, 117, 381–385.

Becker, P. Libowitzky, E., Bohaty, L., Liebertz, J., Rhee, H., Eichler, H.-J., and Kaminskii, A.A. (2012) Temperature-dependent thermo-mechanical and Raman spectroscopy study of the SRS-active melilite-type crystal $Ca_2ZnSi_2O_7$ (hardystonite) at its incommensurate-commensurate phase transition. Physica status solidi (a), 209, 327–334.

Bertaina, S. and Hayn, R. (2006) Exchange integrals and magnetization distribution in $BaCu_2X_2O_7$ (X=Ge,Si). Physical Review B, 73, 212409.

Blass, G., Graf, H.-W., Kolitsch, U., and Sebold, D. (2009) The new finds from the volcanic Eifel (II). Mineralien-Welt, 20, 38–49 (in German).

Blass, G., Schüller, E., and Schüller, W. (2011) "Unglaubliche" Kupfermineralien aus der Vulkaneifel: Auf'm Kopp bei Neroth, Lapis, 22, 21–28, 90 (in German).

Brese, N.E. and O'Keeffe, M. (1991) Bond-valence parameters for solids. Acta Crystallographica, B47, 192–197.

Cannillo, E., Mazzi, F., and Rossi, G. (1988) Crystal structure of andremeyerite, $BaFe(Fe,Mn,Mg)Si_2O_7$. American Mineralogist, 73, 608–612.

Chakoumakos, B.C., Fernandez-Baca, J.A., and Boatner, L.A. (1993) Refinement of the structures of the layer silicates $MCuSi_4O_{10}$ (M=Ca,Sr,Ba) by Rietveld analysis of neutron powder diffraction data. Journal of Solid State Chemistry, 103, 105–113.

Di Domizio, A.J., Downs, R.T., and Yang, H. (2012) Redetermination of clinobarylite, $BaBe_2Si_2O_7$. Acta Crystallographica, E68, i78–i79.

Downs, R.T., Bartelmehs, K.L., Gibbs, G.V., and Boisen, M.B. Jr. (1993) Interactive software for calculating and displaying X-ray or neutron powder diffractometer patterns of crystalline materials. American Mineralogist, 78, 1104–1107.

Finger, L.W., Hazen, R.M., and Hemley, R.J. (1989) $BaCuSi_2O_6$: a new cyclosilicate with four-membered tetrahedral rings. American Mineralogist, 74, 952–955.

Fleet, M.E. and Henderson, G.S. (1997) Structure-composition relations and Raman spectroscopy of high-pressure sodium silicates. Physics and Chemistry of Minerals, 24, 234–355.

Fleet, M.E. and Liu, X. (2001) High-pressure rare earth disilicates $REE_2Si_2O_7$ (REE = Nd, Sm, Eu, Gd): type K. Journal of Solid State Chemistry, 161, 166–172.

Giester, G. and Rieck, B. (1994) Effenbergerite, $BaCu[Si_4O_{10}]$, a new mineral from the Kalahari manganese field, South Africa: description and crystal structure. Mineralogical Magazine, 58, 663–670.

——— (1996) Wesselsite, $SrCu[Si_4O_{10}]$, a further new gillespite-group mineral from the Kalahari Manganese Field, South Africa. Mineralogical Magazine, 60, 795–798.

Gutzmer, J. and Beukes, N.J. (1996) Mineral paragenesis of the Kalahari manganese field, South Africa. Ore Geology Reviews, 11, 405–428.

Hentschel, G. (1993) Die Lavaströme der Graulai: eine neue Fundstelle in der Westeifel. Lapis, 12 (9), 11–23 (in German).

Huang, E., Chen, C.H., Huang, T., Lin, E.H., and Xu, J.-A. (2000) Raman spectroscopic characteristics of Mg-Fe-Ca pyroxenes. American Mineralogist, 85, 473–479.

Janczak, J., Kubiak, R., and Glowiak, T. (1990) Structure of barium copper pyrosilicate at 300 K. Acta Crystallographica, C46, 1383–1385.

Kaminskii, A.A., Rhee, H., Lux, O., Eichler, H.J., Bohaty, L., Becker, P., Liebertz, J., Ueda, K., Shirakawa, A., Voltashev, V.V., Januza, J., Dong, J., and Stavrovskii, D.B. (2011) Many-phonon stimulated Raman scattering and related cascaded and cross-cascaded $\chi^{(3)}$-nonlinear optical effects in melilite-type crystal $Ca_2ZnSi_2O_7$. Laser Physics Letters, 8, 859–874.

Kleyenstuber, A.S.E. (1984) The mineralogy of the manganese-bearing Hotazel Formation, of the Proterozoic Transvaal Sequence in Griqualand West, South Africa. South African Journal of Geology, 87, 257–272.

Knight, K.S., Henderson, C.M.B., and Clark, S.M. (2010) Structural variations in the wesselsite-effenbergerite ($Sr_{1-x}Ba_xCuSi_4O_{10}$) solid solution. European Journal of Mineralogy, 22, 411–423.

Kolitsch, U., Wierzbicka-Wieczorek, M., and Tillmanns, E. (2009) Crystal chemistry and topology of two flux-grown yttrium silicates, $BaKYSi_2O_7$ and $Cs_3YSi_8O_{19}$. Canadian Mineralogist, 47, 421–431.

Krivovichev, S.V., Yakovenchuk, V.N., Armbuster, T., Mikhailova, Y., Pakhomovsky, Y.A. (2004) Clinobarylite, $BaBe_2Si_2O_7$: structure refinement and revision of symmetry and physical properties. Neues Jahrbuch für Mineralogie Monatshefte, 2004, 373–384.

Lin, J.H., Lu, G.X., Du, J., Su, M.Z., Loong, C.-K., and Richardson, J.W. Jr. (1999) Phase transition and crystal structures of $BaZn_2Si_2O_7$. Journal of Physics and Chemistry of Solids, 60, 975–983.

Lu, G.X., Yang, L.Q., and Lin, J.H. (2000) One-dimensional magnetic interaction in $BaMn_2Si_2O_7$. Solid State Communications, 114, 113–116.

Makreski, P., Jovanovski, G., Kaitner, B., Gajovic, A., and Biljan, T. (2007) Minerals from Macedonia XVII. Vibrational spectra of some sorosilicates. Vibrational Spectroscopy, 44, 162–170.

Ohta, H., Okubo, S., Inagaki, Y., Hiroi, Z., Kikuchi, H. (2004a) Recent high field ESR studies of low-dimensional quantum spin systems in Kobe. Physica B, 346–347, 38–44.

Ohta, H., Okubo, S., Fukuoka, D., Inagaki, Y., Kunimoto, T., Kimata, M., Koyama, K., Motokawa, M., Hiroi, Z. (2004b) Breather excitation observed by high-field ESR in one-dimensional antiferromagnet $BaCu_2(Si_{1-x}Ge_x)_2O_7$ (x=0.65). Journal of Magnetism and Magnetic Materials, 272–276, 929–930.

Oliveira, J.A.S. (1993) Crystal-chemical investigations in the systems CuO-BaO-SiO_2-GeO_2 and BaO-Rh_2O_3. Heidelberger Geowissenschaftliche Abhandlungen, 63, 1–185.

Park, C.-H. and Choi, Y.-N. (2009) Crystal structure of $BaMg_2Si_2O_7$ and Eu^{2+} luminescence. Journal of Solid State Chemistry, 182, 1884–1888.

Robinson, P.D. and Fang, J.H. (1977) Barylite, $BaBe_2Si_2O_7$: its space group and

crystal structure. American Mineralogist, 62, 167–169.
Shannon, R.D. (1976) Revised effective ionic radii and systematic studies of interatomic distances in halides and chalcogenides. Acta Crystallographica, A32, 751–767.
Sharma, S.K., Yoder, H.S. Jr., and Matson, D.W. (1988) Raman study of some melilites in crystalline and glassy states. Geochemica et Cosmochemica Acta, 52, 1961–1967.
Sheldrick, G.M. (2008) A short history of *SHELX*. Acta Crystallographica, A64, 112–122.
Sparta, K.M. and Roth, G. (2004) Reinvestigation of the structure of $BaCuSi_2O_6$—evidence for a phase transition at high temperature. Acta Crystallographica, B60, 491–495.
Von Bezing, K.L., Dixon, R.D., Pohl, D., and Cavallo, G. (1991) The Kalahari Manganese Field, an update. Mineralogical Record, 22, 279–297.
Yamada, T., Hiroi, Z., and Takano, M. (2001a) Spin-1/2 quantum antiferromagnetic chains with tunable superexchange interactions found in $BaCu_2(Si_{1-x}Ge_x)_2O_7$. Journal of Solid State Chemistry, 156, 101–109.
Yamada, T., Takano, M., and Hiroi, Z. (2001b) Spin-1/2 quantum antiferromagnetic chains with adjustable superexchange interactions found in $BaCu_2(Si_{1-x}Ge_x)_2O_7$. Journal of Alloys and Compounds, 317–318, 171–176.
Yao, G.Q., Lin, J.H., Zhang, L., Lu, G.X., Gong, M.L., and Su, M.Z. (1998) Luminescent properties of $BaMg_2Si_2O_7$:Eu^{2+}, Mn^{2+}. Journal of Materials Chemistry, 8, 585–588.
Zheludev, A., Masuda, T., Dhalenne, G., Revcolevschi, A., Frost, C., and Perring, T. (2007) Scaling of dynamic spin correlations in $BaCu_2(Si_{0.5}Ge_{0.5})_2O_7$. Physical Review B, 75, 054409.
Zvyagin, A.A. (2006) Effect of doping on the magnetic ordering of quasi-one dimensional antiferromagnets. Low Temperature Physics, 32, 158–161.

Manuscript received August 18, 2012
Manuscript accepted October 7, 2012
Manuscript handled by Fernando Colombo

```
data_scott

_audit_creation_method            SHELXL-97
_chemical_name_systematic
;
 ?
;
_chemical_name_common             ?
_chemical_melting_point           ?
_chemical_formula_moiety          ?
_chemical_formula_sum
 'Ba Cu2 O7 Si2'
_chemical_formula_weight          432.60

loop_
 _atom_type_symbol
 _atom_type_description
 _atom_type_scat_dispersion_real
 _atom_type_scat_dispersion_imag
 _atom_type_scat_source
 'O'  'O'   0.0106   0.0060
 'International Tables Vol C Tables 4.2.6.8 and 6.1.1.4'
 'Si'  'Si'   0.0817   0.0704
 'International Tables Vol C Tables 4.2.6.8 and 6.1.1.4'
 'Cu'  'Cu'   0.3201   1.2651
 'International Tables Vol C Tables 4.2.6.8 and 6.1.1.4'
 'Ba'  'Ba'  -0.3244   2.2819
 'International Tables Vol C Tables 4.2.6.8 and 6.1.1.4'

_symmetry_cell_setting            ?
_symmetry_space_group_name_H-M    ?

loop_
 _symmetry_equiv_pos_as_xyz
 'x, y, z'
 '-x+1/2, -y, z+1/2'
 '-x, y+1/2, -z'
 'x+1/2, -y+1/2, -z+1/2'
 '-x, -y, -z'
 'x-1/2, y, -z-1/2'
 'x, -y-1/2, z'
 '-x-1/2, y-1/2, z-1/2'

_cell_length_a                    6.8556(2)
_cell_length_b                    13.1725(4)
_cell_length_c                    6.8901(2)
_cell_angle_alpha                 90.00
_cell_angle_beta                  90.00
_cell_angle_gamma                 90.00
_cell_volume                      622.21(3)
_cell_formula_units_Z             4
_cell_measurement_temperature     293(2)
_cell_measurement_reflns_used     ?
_cell_measurement_theta_min       ?
```

```
_cell_measurement_theta_max       ?

_exptl_crystal_description        ?
_exptl_crystal_colour             ?
_exptl_crystal_size_max           ?
_exptl_crystal_size_mid           ?
_exptl_crystal_size_min           ?
_exptl_crystal_density_meas       ?
_exptl_crystal_density_diffrn     4.618
_exptl_crystal_density_method     'not measured'
_exptl_crystal_F_000              792
_exptl_absorpt_coefficient_mu     13.409
_exptl_absorpt_correction_type    ?
_exptl_absorpt_correction_T_min   ?
_exptl_absorpt_correction_T_max   ?
_exptl_absorpt_process_details    ?

_exptl_special_details
;
 ?
;

_diffrn_ambient_temperature       293(2)
_diffrn_radiation_wavelength      0.71073
_diffrn_radiation_type            MoK\a
_diffrn_radiation_source          'fine-focus sealed tube'
_diffrn_radiation_monochromator   graphite
_diffrn_measurement_device_type   ?
_diffrn_measurement_method        ?
_diffrn_detector_area_resol_mean  ?
_diffrn_standards_number          ?
_diffrn_standards_interval_count  ?
_diffrn_standards_interval_time   ?
_diffrn_standards_decay_%         ?
_diffrn_reflns_number             4887
_diffrn_reflns_av_R_equivalents   0.0232
_diffrn_reflns_av_sigmaI/netI     0.0196
_diffrn_reflns_limit_h_min        -10
_diffrn_reflns_limit_h_max        8
_diffrn_reflns_limit_k_min        -19
_diffrn_reflns_limit_k_max        19
_diffrn_reflns_limit_l_min        -10
_diffrn_reflns_limit_l_max        7
_diffrn_reflns_theta_min          3.09
_diffrn_reflns_theta_max          32.56
_reflns_number_total              1180
_reflns_number_gt                 1065
_reflns_threshold_expression      >2sigma(I)

_computing_data_collection        ?
_computing_cell_refinement        ?
_computing_data_reduction         ?
_computing_structure_solution     'SHELXS-97 (Sheldrick, 1990)'
_computing_structure_refinement   'SHELXL-97 (Sheldrick, 1997)'
_computing_molecular_graphics     ?
```

```
_computing_publication_material   ?

_refine_special_details
;
 Refinement of F^2^ against ALL reflections.  The weighted R-factor wR and
 goodness of fit S are based on F^2^, conventional R-factors R are based
 on F, with F set to zero for negative F^2^. The threshold expression of
 F^2^ > 2sigma(F^2^) is used only for calculating R-factors(gt) etc. and is
 not relevant to the choice of reflections for refinement.  R-factors based
 on F^2^ are statistically about twice as large as those based on F, and R-
 factors based on ALL data will be even larger.
;

_refine_ls_structure_factor_coef  Fsqd
_refine_ls_matrix_type            full
_refine_ls_weighting_scheme       calc
_refine_ls_weighting_details
 'calc w=1/[\s^2^(Fo^2^)+(0.0212P)^2^+0.0000P] where P=(Fo^2^+2Fc^2^)/3'
_atom_sites_solution_primary      direct
_atom_sites_solution_secondary    difmap
_atom_sites_solution_hydrogens    geom
_refine_ls_hydrogen_treatment     mixed
_refine_ls_extinction_method      none
_refine_ls_extinction_coef        ?
_refine_ls_number_reflns          1180
_refine_ls_number_parameters      58
_refine_ls_number_restraints      0
_refine_ls_R_factor_all           0.0206
_refine_ls_R_factor_gt            0.0174
_refine_ls_wR_factor_ref          0.0407
_refine_ls_wR_factor_gt           0.0398
_refine_ls_goodness_of_fit_ref    1.074
_refine_ls_restrained_S_all       1.074
_refine_ls_shift/su_max           0.000
_refine_ls_shift/su_mean          0.000

loop_
 _atom_site_label
 _atom_site_type_symbol
 _atom_site_fract_x
 _atom_site_fract_y
 _atom_site_fract_z
 _atom_site_U_iso_or_equiv
 _atom_site_adp_type
 _atom_site_occupancy
 _atom_site_symetry_multiplicity
 _atom_site_calc_flag
 _atom_site_refinement_flags
 _atom_site_disorder_assembly
 _atom_site_disorder_group
Ba Ba 0.01303(2) 0.2500 0.45688(3) 0.00971(5) Uani 1 2 d S . .
Cu Cu 0.27762(4) 0.004172(18) 0.20631(4) 0.00714(6) Uani 1 1 d . . .
Si Si 0.49765(7) 0.13406(5) 0.52716(8) 0.00567(11) Uani 1 1 d . . .
O1 O 0.4044(3) 0.2500 0.5167(3) 0.0087(4) Uani 1 2 d S . .
O2 O 0.1725(2) 0.13369(11) 0.1306(2) 0.0104(3) Uani 1 1 d . . .
```

```
O3 O 0.5590(2) 0.11214(12) 0.7486(2) 0.0111(3) Uani 1 1 d . . .
O4 O 0.3173(2) 0.05957(12) 0.4658(2) 0.0078(3) Uani 1 1 d . . .

loop_
 _atom_site_aniso_label
 _atom_site_aniso_U_11
 _atom_site_aniso_U_22
 _atom_site_aniso_U_33
 _atom_site_aniso_U_23
 _atom_site_aniso_U_13
 _atom_site_aniso_U_12
Ba 0.00886(8) 0.01080(9) 0.00946(9) 0.000 -0.00075(6) 0.000
Cu 0.00894(11) 0.00574(11) 0.00675(12) -0.00084(9) -0.00225(8) 0.00142(8)
Si 0.0066(2) 0.0047(2) 0.0057(2) -0.00003(19) 0.00040(19) 0.00039(17)
O1 0.0084(9) 0.0057(9) 0.0120(10) 0.000 -0.0004(8) 0.000
O2 0.0121(6) 0.0068(7) 0.0122(7) -0.0003(6) -0.0053(6) 0.0022(5)
O3 0.0152(7) 0.0098(7) 0.0083(7) -0.0017(6) -0.0031(6) 0.0048(5)
O4 0.0105(6) 0.0076(7) 0.0053(6) -0.0010(5) 0.0007(5) -0.0022(5)

_geom_special_details
;
 All esds (except the esd in the dihedral angle between two l.s. planes)
 are estimated using the full covariance matrix.  The cell esds are taken
 into account individually in the estimation of esds in distances, angles
 and torsion angles; correlations between esds in cell parameters are only
 used when they are defined by crystal symmetry.  An approximate (isotropic)
 treatment of cell esds is used for estimating esds involving l.s. planes.
;

loop_
 _geom_bond_atom_site_label_1
 _geom_bond_atom_site_label_2
 _geom_bond_distance
 _geom_bond_site_symmetry_2
 _geom_bond_publ_flag
Ba O1 2.715(2) . ?
Ba O3 2.7413(16) 4_456 ?
Ba O3 2.7413(15) 6_557 ?
Ba O2 2.8569(15) 6_556 ?
Ba O2 2.8569(15) 4_455 ?
Ba O2 2.9320(16) . ?
Ba O2 2.9320(16) 7_565 ?
Ba O4 3.2629(15) 7_565 ?
Ba O4 3.2629(15) . ?
Ba Si 3.6696(6) 6_556 ?
Ba Si 3.6696(6) 4_455 ?
Ba Si 3.6885(6) 7_565 ?
Cu O3 1.9231(15) 5_656 ?
Cu O2 1.9243(15) . ?
Cu O4 1.9502(15) . ?
Cu O4 1.9682(15) 2_554 ?
Cu Si 2.8983(6) 2_554 ?
Cu Ba 3.7888(3) 6_656 ?
Si O3 1.6089(17) . ?
Si O2 1.6178(16) 6_656 ?
```

```
Si O4 1.6342(16) . ?
Si O1 1.6572(10) . ?
Si Cu 2.8983(6) 2 ?
Si Ba 3.6696(6) 6_656 ?
O1 Si 1.6572(10) 7_565 ?
O2 Si 1.6178(16) 6_556 ?
O2 Ba 2.8569(15) 6_656 ?
O3 Cu 1.9231(15) 5_656 ?
O3 Ba 2.7413(15) 6_657 ?
O4 Cu 1.9682(15) 2 ?

loop_
 _geom_angle_atom_site_label_1
 _geom_angle_atom_site_label_2
 _geom_angle_atom_site_label_3
 _geom_angle
 _geom_angle_site_symmetry_1
 _geom_angle_site_symmetry_3
 _geom_angle_publ_flag
O1 Ba O3 76.93(5) . 4_456 ?
O1 Ba O3 76.93(5) . 6_557 ?
O3 Ba O3 82.97(7) 4_456 6_557 ?
O1 Ba O2 147.12(3) . 6_556 ?
O3 Ba O2 127.25(4) 4_456 6_556 ?
O3 Ba O2 83.97(5) 6_557 6_556 ?
O1 Ba O2 147.12(3) . 4_455 ?
O3 Ba O2 83.97(5) 4_456 4_455 ?
O3 Ba O2 127.25(4) 6_557 4_455 ?
O2 Ba O2 64.86(6) 6_556 4_455 ?
O1 Ba O2 75.41(5) . . ?
O3 Ba O2 150.56(4) 4_456 . ?
O3 Ba O2 100.29(4) 6_557 . ?
O2 Ba O2 82.11(4) 6_556 . ?
O2 Ba O2 115.03(3) 4_455 . ?
O1 Ba O2 75.41(5) . 7_565 ?
O3 Ba O2 100.29(4) 4_456 7_565 ?
O3 Ba O2 150.56(4) 6_557 7_565 ?
O2 Ba O2 115.03(3) 6_556 7_565 ?
O2 Ba O2 82.11(4) 4_455 7_565 ?
O2 Ba O2 63.00(6) . 7_565 ?
O1 Ba O4 50.60(3) . 7_565 ?
O3 Ba O4 53.36(4) 4_456 7_565 ?
O3 Ba O4 114.95(4) 6_557 7_565 ?
O2 Ba O4 159.83(4) 6_556 7_565 ?
O2 Ba O4 96.55(4) 4_455 7_565 ?
O2 Ba O4 100.25(4) . 7_565 ?
O2 Ba O4 51.28(4) 7_565 7_565 ?
O1 Ba O4 50.60(3) . . ?
O3 Ba O4 114.95(4) 4_456 . ?
O3 Ba O4 53.36(4) 6_557 . ?
O2 Ba O4 96.55(4) 6_556 . ?
O2 Ba O4 159.83(4) 4_455 . ?
O2 Ba O4 51.28(4) . . ?
O2 Ba O4 100.25(4) 7_565 . ?
O4 Ba O4 100.49(5) 7_565 . ?
```

```
O1 Ba Si 99.58(4) . 6_556 ?
O3 Ba Si 162.13(3) 4_456 6_556 ?
O3 Ba Si 113.60(3) 6_557 6_556 ?
O2 Ba Si 64.00(3) 6_556 6_556 ?
O2 Ba Si 90.46(3) 4_455 6_556 ?
O2 Ba Si 25.36(3) . 6_556 ?
O2 Ba Si 62.05(3) 7_565 6_556 ?
O4 Ba Si 110.82(3) 7_565 6_556 ?
O4 Ba Si 73.47(3) . 6_556 ?
O1 Ba Si 99.58(4) . 4_455 ?
O3 Ba Si 113.60(3) 4_456 4_455 ?
O3 Ba Si 162.13(3) 6_557 4_455 ?
O2 Ba Si 90.46(3) 6_556 4_455 ?
O2 Ba Si 64.00(3) 4_455 4_455 ?
O2 Ba Si 62.05(3) . 4_455 ?
O2 Ba Si 25.36(3) 7_565 4_455 ?
O4 Ba Si 73.47(3) 7_565 4_455 ?
O4 Ba Si 110.82(3) . 4_455 ?
Si Ba Si 49.189(19) 6_556 4_455 ?
O1 Ba Si 24.464(9) . 7_565 ?
O3 Ba Si 61.64(3) 4_456 7_565 ?
O3 Ba Si 94.22(4) 6_557 7_565 ?
O2 Ba Si 170.36(3) 6_556 7_565 ?
O2 Ba Si 122.81(3) 4_455 7_565 ?
O2 Ba Si 88.93(3) . 7_565 ?
O2 Ba Si 63.16(3) 7_565 7_565 ?
O4 Ba Si 26.29(3) 7_565 7_565 ?
O4 Ba Si 74.94(3) . 7_565 ?
Si Ba Si 108.514(14) 6_556 7_565 ?
Si Ba Si 88.445(14) 4_455 7_565 ?
O3 Cu O2 165.55(7) 5_656 . ?
O3 Cu O4 93.95(7) 5_656 . ?
O2 Cu O4 88.23(6) . . ?
O3 Cu O4 89.34(6) 5_656 2_554 ?
O2 Cu O4 91.49(6) . 2_554 ?
O4 Cu O4 167.84(3) . 2_554 ?
O3 Cu Si 86.99(5) 5_656 2_554 ?
O2 Cu Si 101.39(5) . 2_554 ?
O4 Cu Si 135.75(5) . 2_554 ?
O4 Cu Si 32.68(4) 2_554 2_554 ?
O3 Cu Ba 118.74(5) 5_656 6_656 ?
O2 Cu Ba 47.26(5) . 6_656 ?
O4 Cu Ba 83.85(4) . 6_656 ?
O4 Cu Ba 104.80(4) 2_554 6_656 ?
Si Cu Ba 133.463(15) 2_554 6_656 ?
O3 Si O2 116.29(8) . 6_656 ?
O3 Si O4 109.60(9) . . ?
O2 Si O4 112.65(8) 6_656 . ?
O3 Si O1 107.90(10) . . ?
O2 Si O1 105.03(9) 6_656 . ?
O4 Si O1 104.49(9) . . ?
O3 Si Cu 69.74(6) . 2 ?
O2 Si Cu 140.05(6) 6_656 2 ?
O4 Si Cu 40.56(5) . 2 ?
O1 Si Cu 110.26(7) . 2 ?
```

```
O3 Si Ba 158.29(6) . 6_656 ?
O2 Si Ba 50.91(6) 6_656 6_656 ?
O4 Si Ba 92.10(6) . 6_656 ?
O1 Si Ba 65.67(8) . 6_656 ?
Cu Si Ba 131.855(18) 2 6_656 ?
O3 Si Ba 115.74(6) . . ?
O2 Si Ba 125.47(6) 6_656 . ?
O4 Si Ba 62.16(6) . . ?
O1 Si Ba 42.72(7) . . ?
Cu Si Ba 74.310(12) 2 . ?
Ba Si Ba 74.588(11) 6_656 . ?
Si O1 Si 134.32(13) 7_565 . ?
Si O1 Ba 112.82(7) 7_565 . ?
Si O1 Ba 112.82(7) . . ?
Si O2 Cu 117.54(9) 6_556 . ?
Si O2 Ba 117.53(8) 6_556 6_656 ?
Cu O2 Ba 103.09(6) . 6_656 ?
Si O2 Ba 103.74(7) 6_556 . ?
Cu O2 Ba 113.26(7) . . ?
Ba O2 Ba 100.73(5) 6_656 . ?
Si O3 Cu 116.64(9) . 5_656 ?
Si O3 Ba 123.58(8) . 6_657 ?
Cu O3 Ba 118.37(7) 5_656 6_657 ?
Si O4 Cu 124.56(9) . . ?
Si O4 Cu 106.77(8) . 2 ?
Cu O4 Cu 124.49(8) . 2 ?
Si O4 Ba 91.55(6) . . ?
Cu O4 Ba 100.44(6) . . ?
Cu O4 Ba 97.62(5) 2 . ?

_diffrn_measured_fraction_theta_max    0.997
_diffrn_reflns_theta_full              32.56
_diffrn_measured_fraction_theta_full   0.997
_refine_diff_density_max    1.517
_refine_diff_density_min   -0.672
_refine_diff_density_rms    0.162
```